On-sky experiment of the discrete beam combiner: lessons learned and strategies for improved calibration of the transfer function

Abani Shankar Nayak, Lucas Labadie, Tarun Sharma,

Simone Piacentini, Giacomo Corrielli, et al.

Published version information:

Citation: AS Nayak et al. On-sky experiment of the discrete beam combiner: lessons learned and strategies for improved calibration of the transfer function. Proc SPIE 12183 (2022): 121832H. Is in proceedings of: Conference on Optical and Infrared Interferometry and Imaging VIII Part of SPIE Astronomical Telescopes and Instrumentation Conference, Montreal, CANADA, 17-22 Jul 2022

DOI: 10.1117/12.2629673

On-sky experiment of the discrete beam combiner: lessons learned and strategies for improved calibration of the transfer function

Abani Shankar Nayak, Lucas Labadie, Tarun Sharma, Simone Piacentini, Giacomo Corrielli, et al.

Abani Shankar Nayak, Lucas Labadie, Tarun K. Sharma, Simone Piacentini, Giacomo Corrielli, Roberto Osellame, Ettore Pedretti, Aline N. Dinkelaker, Eloy Hernandez, Kalaga V. Madhav, Martin M. Roth, "On-sky experiment of the discrete beam combiner: lessons learned and strategies for improved calibration of the transfer function," Proc. SPIE 12183, Optical and Infrared Interferometry and Imaging VIII, 121832H (26 August 2022); doi: 10.1117/12.2629673

SPIE.

Event: SPIE Astronomical Telescopes + Instrumentation, 2022, Montréal, Québec, Canada

On-sky experiment of the discrete beam combiner: lessons learned and strategies for improved calibration of the transfer function

Abani Shankar Nayak[a], Lucas Labadie[b], Tarun K. Sharma[b], Simone Piacentini[c,d], Giacomo Corrielli[d,c], Roberto Osellame[d,c], Ettore Pedretti[e], Aline N. Dinkelaker[a], Eloy Hernandez[a], Kalaga V. Madhav[a], and Matin M. Roth[a]

[a]Leibniz-Institut für Astrophysik Potsdam, An der Sternwarte 16, 14482 Potsdam, Germany
[b]1. Physikalisches Institut Uni Köln, Zülpicher Str. 77, 50937 Köln, Germany
[c]Dipartimento di Fisica, Politecnico di Milano, Piazz L. da Vinci 32, 20133 Milano, Italy
[d]Istituto di Fotonica e Nanotecnologie – CNR, Piazza L. da Vinci 21, 20133 Milano, Italy
[e]STFC Rutherford Appleton Lab., Harwell Campus, Didcot, UK

ABSTRACT

We recently performed tests of the discrete beam combiner (DBC) through an on-sky experiment using a 4-input pupil remappers-based integrated optics device. Here, we report on the lessons learned, as well as visibilities and closure phase results for our stellar target, Vega. Through complementary simulations, we analyze how the residual phase errors, input power imbalance at the waveguides, slow environmental changes, and different photon levels affect the performance of the DBC. This is an important aspect to improve future on-sky calibration strategies for this type of beam combiner, in particular when combining a large number of apertures.

Keywords: Long baseline interferometry, beam combiners, interferometric visibility, closure phase, integrated optics, ultra-fast laser inscription, pupil remapping, on-sky experiment

1. INTRODUCTION

A discrete beam combiner (DBC) consists of a photonic lattice, an array of single-mode waveguides that weakly interact with each other through evanescent fields. DBC have found applications in creation of discrete solitons,[1] generation of discrete diffraction,[2] propagation of surface states[3] and generation of vortex states of light,[4] but Minardi & Pertsch[5] are usually credited for developing this concept in the context of long-baseline interferometry. Following their works, various architectures of DBC consisting of N-input/M-output waveguides (WGs) arranged in hexagonal,[6] square[7] and zig-zag[8] lattices were numerically studied. The experimental verification of retrieving interferometric visibilities from the DBC was also demonstrated at astronomical R,[9] J,[10] and L[8]-bands.

The interferometric visibilities can be retrieved from the DBC through a matrix $\{U\}$, known as the transfer matrix of the DBC, which describes the interaction of the single-mode waveguides in the array. Once $\{U\}$ is obtained either in the design or the characterization step, the visibilities are extracted by calculating the power/photometry at the output waveguides of the DBC. The matrix $\{U\}$ contains the coherence terms (see Ref. 8, 11 for details), namely the self-coherence terms (Γ_{ii}) and mutual coherence terms (Γ_{ij}) from where the visibility information of the light source is obtained. It was found that visibilities extracted from the DBC have fewer biases to external phase errors if a next-nearest neighbour coupling[12] between the single-mode waveguides is ensured along the interaction length of the DBC, which was also verified experimentally.[8,10,11]

Due to the 3-dimensional (3D) design of the DBC, these structures are usually fabricated using the method of ultra-fast laser inscription (ULI).[13] The 3D capability of this manufacturing technology have led to the realization of 4-input pupil remappers,[14,15] DBC and 23-output coherent reformatters[16,17] in a single monolithic integrated optics (IO) chip to be operated at H-band (1.6 μm).[18] The successful fabrication of this IO chip was due to recent

Further author information: (Send correspondence to A.S.N.)
A.S.N.: E-mail: anayak@aip.de, Telephone: +49 331 7499 447

Optical and Infrared Interferometry and Imaging VIII, edited by Antoine Mérand, Stephanie Sallum, Joel Sanchez-Bermudez,
Proc. of SPIE Vol. 12183, 121832H · © 2022 SPIE · 0277-786X · doi: 10.1117/12.2629673

advances both in the manufacturing technology and the device itself, which included low birefringence of single-mode waveguides,[19] good coupling of input reformatters with standard single-mode fibers, and a bandwidth study of the DBC.[11] After laboratory characterization of different DBC devices, the next step was to operate the DBC under realistic observing conditions, which was done recently at the William Herschel Telescope (WHT) through a pupil remapping experiment.[20] In the experiment, we successfully coupled starlight into the device from targets such as Vega and Altair. We retrieved the visibility amplitude and closure phase (CP), but with significant dispersion that was recently published in Ref. 21. Though most of the analysis was presented in Ref. 21, in this proceeding, we attempted to look further at our on-sky experimental layout by studying the input power imbalance and phase errors at the DBC and at different photon levels. This kind of study will better prepare us for further on-sky tests of the DBC, in particular when combining a large number of apertures. Thus, in Sec. 2, we briefly describe the experimental layout, and Sec. 3 shows the on-sky visibilities obtained for Vega. Finally, Sec. 4 shows the simulation results of the DBC to power imbalance and phase errors.

2. EXPERIMENTAL LAYOUT AT THE WILLIAM HERSCHEL TELESCOPE

The pupil remapping experiment was performed on the Nasmyth platform of the WHT from the nights of 9–12 August 2019. The schematic layout of the setup that was used to couple stellar light into the IO device is shown in Fig. 1. We require two important optical components for such a pupil remapping experiment:[15,22] 1) Segmented mirror (SM) and 2) Micro lens array (MLA). The segmented mirror is used such that the telescope pupil reimages on its hexagonal segments. In our setup, the SM was used only for static injection of the sub-pupils into their corresponding pupil remappers. We assumed that the f/11 beam coming after the adaptive optics system of the WHT (called CANARY[23,24]) was planar enough that our SM required no active stabilization. The role of the MLA is to efficiently couple light into the pupil remappers. In ideal conditions, a coupling efficiency of 80% can be reached between the lenslet of the MLA and the single-mode WGs of the pupil remappers. Fig. 1b shows the 1:1 optical conjugation of the SM with the MLA, where 37 focal spots are formed on the focal plane. The other optical components of the setup (e.g., mirrors and lenses) were chosen in such a way that the 1.2 m obscuration of the WHT projects a diameter of 0.625 mm, and the 4.2 m primary mirror of the WHT projects a diameter of 2.125 mm on the focal plane of the MLA.

We used our own internal calibration source to obtain the transfer matrix $\{U\}$ of the system. The optical transfer matrix was obtained by launching light into the optical path consisting of all the optical components after the Nasmyth focus, which also included the WHT adaptive optics system, CANARY. Before obtaining the transfer matrix, the setup shown in Fig. 1 was aligned to couple light from the calibration source into the IO chip. This alignment procedure included adjusting the three degrees of freedom (i.e., tip/tilt/piston) of the individual segments of the SM by observing the maximum intensity change at the output facet when one of the focal spots highlighted in Fig. 1b is steered into the optical path. During this alignment step, the deformable mirror of the CANARY system corresponds to a close to a flat configuration. The tip/tilt/piston information of the individual segments of the SM was then used for obtaining the $\{U\}$ of the system and also to successfully couple starlight into the IO device during our night observations.

We used two InGaAs cameras at that time: Ninox640 from Raptor photonics and CRED2 from FIRST Light. We used the Ninox640 for alignment and obtaining the $\{U\}$ matrix since we had the software for synchronous control that is necessary to obtain a robust $\{U\}$. We used the CRED2 during our night observations due to its lower dark current and readout noise. However, unfortunately, we did not have software for synchronous control of the CRED2 and the SM, which prevented us from performing a suitable calibration and obtaining the $\{U\}$ matrix with this camera. A summation of 5 pixels, as highlighted in Fig. 1c, was used to extract the power at the output waveguides of the DBC. The extracted power information forms the base for obtaining both the $\{U\}$ and the on-sky visibilities. All frames were bias subtracted to measure the power at the outputs of the DBC. The bias frames were recorded by blocking the light before L1 as shown in Fig. 1 with a physical aperture.

3. ON-SKY VISIBILITIES

The CRED2 camera used during the on-sky observations was water-cooled down to 233 K to reduce the thermal noise of the sensor. As highlighted in Fig. 1b, the four focal spots were used to couple light into the IO device.

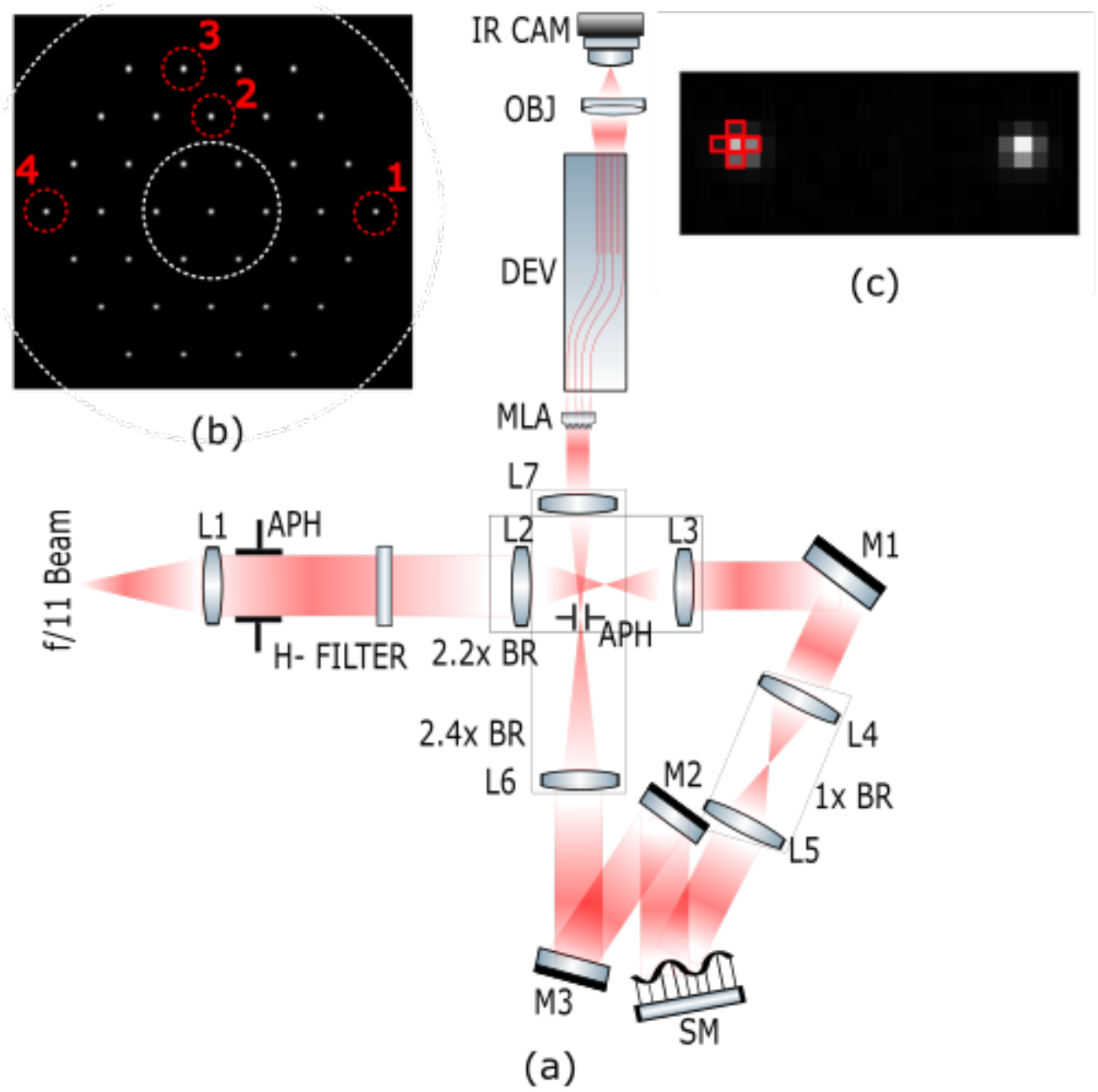

Figure 1. *(not to scale)* (a) The schematic of the optical setup that was used for the pupil remapping experiment at the WHT. Following are the acronyms: f/11 beam: AO corrected beam of the WHT; L: lens; APH: adjustable pin hole; H-filter: band pass filter centered at 1600 nm with a bandwidth of 50 nm; BR: beam reducer; M: mirror; SM: segmented mirror; MLA: micro lens array; DEV: integrated optics device; OBJ: objective; IR CAM: infrared camera. (b) The 37 focal spots formed at the focal plane of the MLA show the 1:1 conjugation between the individual segments of the SM and the lenslets of the MLA. The four focal spots that will couple light into the 4-input pupil remappers are highlighted in red. The inner and outer circles show the projection of the obscuration (0.625 mm) and the primary mirror (2.125 mm) of the WHT, respectively, on the focal plane of the MLA. (c) For clarity, two of the output waveguides of the DBC recorded by the camera are shown. The red augmented area consisting of 5 pixels is also shown, which is used for extracting the power from the output waveguides of the DBC.

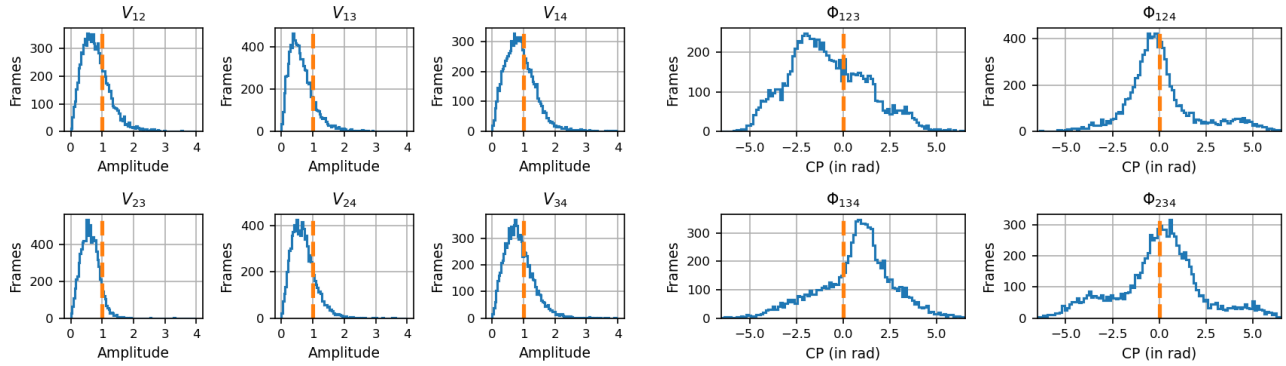

(a) (b)

Figure 2. Histogram plots showing the retrieved visibilities (in blue) of Vega for all baselines. The orange line shows the theoretical value, and the y-axis shows the number of camera frames. Large deviations around the theoretical values are seen. (a) Visibility amplitude. (b) Closure phase.

The remaining 33 focal spots were moved out of the optical path by adjusting the individual segments of the SM, with the parameters identified during the alignment step described in Sec. 2. With the setup shown in Fig. 1, the IO device containing both the pupil remappers and the DBC received its first stellar photons from Vega. During the on-sky observation, the exposure time (t_e) of the CRED2 camera was set to 250 ms at high gain mode. This value was chosen as a compromise between increasing the SNR and decreasing the decoherence effects of the atmosphere. As we were not in a position to analyze the real-time wavefront corrections provided by CANARY, we adopted this t_e value from a similar pupil remapping experiment at H-band.[15] Please note that in our on-sky experiment, there was no temporal scanning (i.e., no path delay was applied) in the segments of the SM. We recorded a series of camera frames by passively injecting all four focal spots into the IO chip. The frames recorded were bias-subtracted, and the output power at the waveguides of the DBC was extracted. The power extracted from the observation of Vega was applied to the $\{U\}$ of the system obtained in Sec. 2 to retrieve the visibilities. The on-sky visibilities obtained from Vega are shown as histogram plots on how the number of camera frames contributes both to the amplitude value in Fig. 2a and to the CP value in Fig. 2b. We see that there are large deviations around the theoretical values expected for a point source, $V_{ij} \sim 1$ and $\Phi_{ijk} \sim 0$. Similar deviations were obtained for Altair and can be found in Tab. 4 of Ref. 21.

In order to understand these deviations, we did a comparable simulation using the commercially available software BeamPROP from Rsoft. We found out that the main reason for such deviations was caused by the photon noise limit. With an effective single aperture of $\sim$ 50 cm, the choice of our value for t_e, moderate SNR values of 2–14 reported from the experiment, and an upper limit of 4 % throughput of our overall system, we ended up in a photon starved regime. At such a photon limit, the detector noise of the CRED2 camera also played a very important role in shifting the peak of the histogram away from the expected values. It was found that when the readout noise was set to 22 e^- and the dark current value was set to 600 e^-/s/pixel at high gain mode in the simulations, a spread in the histogram is seen. Thus, both the peaks and the shape of the histogram are affected by a combination of photon and detector noise. It is also to be noted that two different detectors were used in the experiment. Though the pixel dimensions are the same for both cameras, the noise values are different. As a result, this might be detrimental in estimating robust on-sky visibilities. The choice of t_e for the experiment might also have been too long and therefore impacted the results. It was found that at the level of Strehl ratio (SR) offered by the CANARY and the coherence time of the atmosphere, such t_e value leads to a decrease in the visibility value, thus shifting the peak of the histograms.

All of the above findings were reported in Ref. 21. However, the effect of the visibilities due to photometry imbalance reported in Tab. 5 of Ref. 21 was not fully understood. In the next section, we will show our findings through simulation.

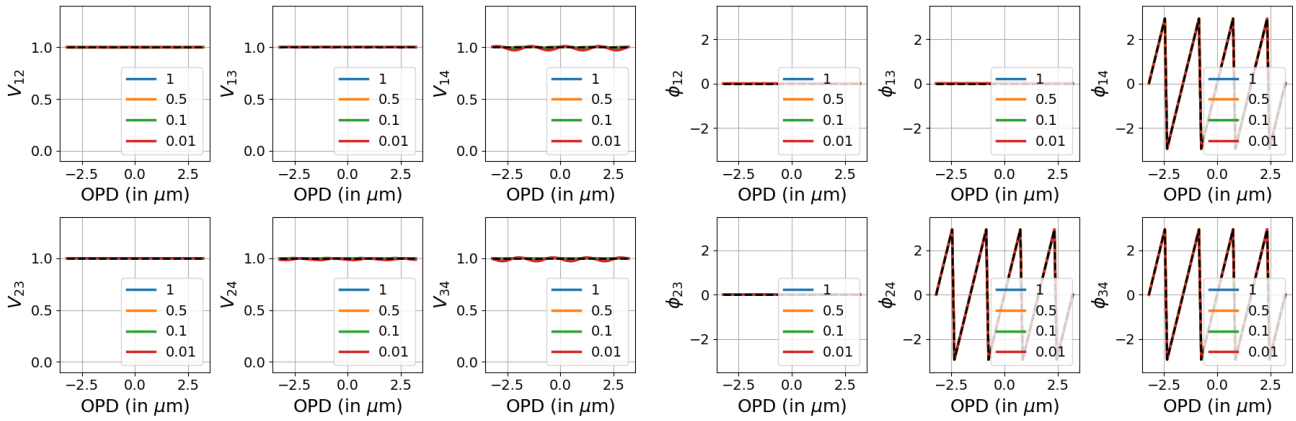

(a) (b)

Figure 3. Retrieved visibilities from the DBC where a phase ramp is applied to input number 4. Black is the theoretical value. The legend shows the factor that was applied to vary the amplitude of the input waveguide numbered 4. The factor of 1 represents no variation in the input amplitude, which corresponds to the case of equal amplitude in all input waveguides of the DBC. (a) Visibility amplitude. (b) Visibility phase. Since there is a linear phase ramp at input numbered 4, we observe the retrieved phase of ϕ_{14}, ϕ_{24} and ϕ_{34} to follow the same pattern.

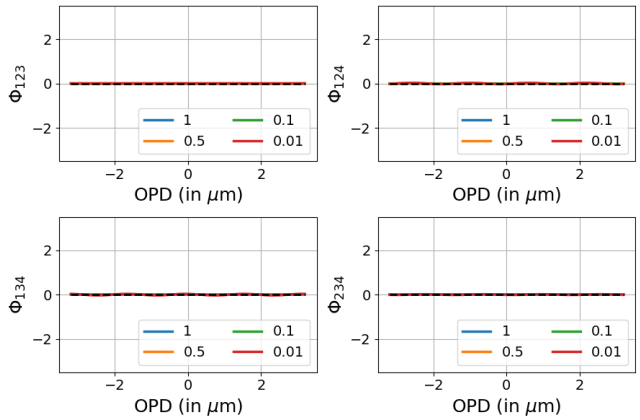

Figure 4. The resilient behaviour of the retrieved closure phase (in blue) to external phase errors is seen that matches well with the theoretical prediction in black. The legend shows the factor that was applied to vary the amplitude of input waveguide numbered 4, where a factor of 1 represents no variation.

4. SIMULATION

The DBC was simulated in Rsoft with the parameters that were very close to those obtained from the fabricated device. In the simulation setup, four electric fields with Gaussian profiles were launched into the DBC. In one of the arms – input numbered 4, a passive variation in the amplitude value (i.e. a factor of 1, $\frac{1}{2}$, $\frac{1}{10}$ and $\frac{1}{100}$) and a dynamic variation in the phase (i.e. applied path difference) in form of a linear ramp is applied. A sequence of images was obtained in the process, the power at the output waveguides was extracted and applied to the calibrated $\{U\}$ obtained from the simulation at 1600 nm. The results of the visibilities and the CP are shown in Fig. 3 and Fig. 4, respectively as a function of applied optical path difference (OPD). It is seen that for all baselines $V_{ij} \sim 1$, $\phi_{ij} \sim 0$ except where a linear phase ramp is applied at the input, and $\Phi_{ijk} \sim 0$, which perfectly matches with the theoretical curve shown in black. From the figures, it can be concluded that in an ideal situation consisting of a photon-rich regime and noiseless detectors, the accuracy of the retrieved visibilities and CP have unprecedented levels, independent of the amplitude or phase variation at the input waveguides of the DBC.

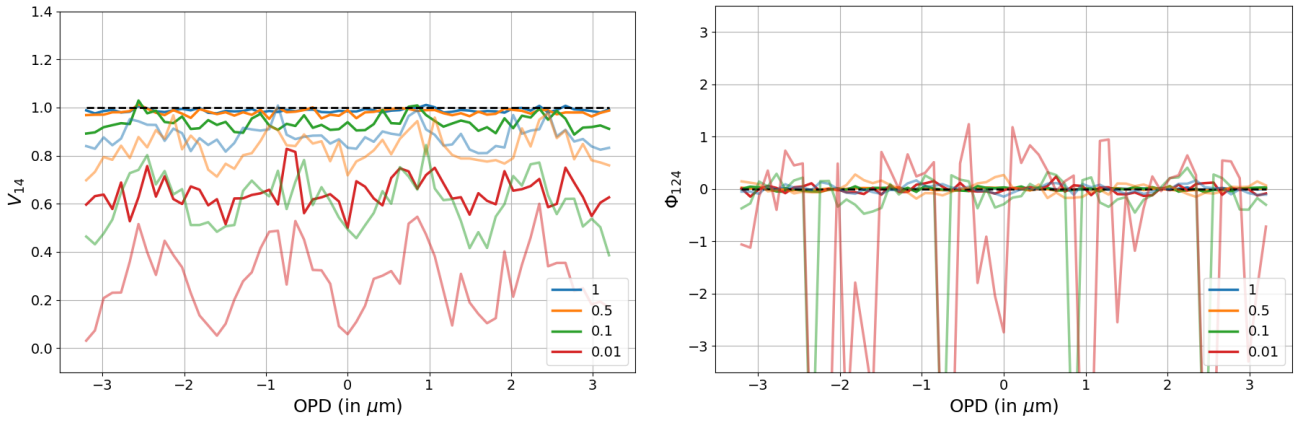

(a) (b)

Figure 5. Retrieved visibilities from the DBC for the situation shown in Figs. 3 and 4 along with added photon and detector noise. Black is the theoretical value. Dark color represents a high-photon regime, and light color represents an intermediate-photon regime. The legend shows the factor with which the amplitude of the input waveguide numbered 4 was varied. The factor of 1 represents no variation in the input amplitude, which corresponds to the case of equal amplitude in all input waveguides of the DBC. (a) Visibility amplitude. (b) Closure phase.

Next, we will consider the presence of photon noise and the level of detector noise that was present during our on-sky test, as reported in Sec. 3. Since the output images obtained from Rsoft are normalized, we multiplied it by a constant factor to convert the pixels of the images into the number of photons. Successively, we added photon noise and detector noises in the form of readout noise (22 e^-) and dark current (150 e^-/pixel). We then converted the pixel values into 14-bit camera counts, which is what was obtained from the CRED2 camera. While adding the photon noise, we considered three scenarios: 1) High-photon regime corresponding to 10^5 photons/pixel to avoid any saturation value* in the simulated images, 2) Low-photon regime corresponding to 10^3 photons/pixel, which consists of more background noise than the coherent signal and 3) Intermediate-photon regime corresponding to 10^4 photons/pixel that corresponds to photon levels observed during the on-sky test. For clarity, we will show only one visibility pair (i.e., V_{14}) and 1 CP (i.e., Φ_{124}) in the subsequent analysis. This pair and triplet choice were made randomly from a set of baseline pairs with a linear phase ramp at the input. The visibility amplitude and CP are shown in Fig. 5a and Fig. 5b, respectively. To show the trend, we show the case of the high-photon regime in dark color and the intermediate-photon regime in a light color. It was found that in the high-photon regime, the accuracy of visibility amplitude retrieval decreases from 98.8 % to 64.5 % as the photometry imbalance at the input waveguides of the DBC increases.

Similarly, in the high-photon regime, the standard deviation of CP increases† from 0.01 rad to 0.08 rad as the photometry imbalance increases. However, in the intermediate-photon regime, both the accuracy of the visibility amplitude and the precision of CP retrieved from the DBC were severely affected. This shows that operating at low photon numbers could have detrimental effects on achieving high accuracy visibilities and high precision CP for the DBC.

In order to better understand these results, we will analyze the retrieved input photometries from the DBC. As the coherence functions from the DBC can be simultaneously retrieved, the self-coherence terms (i.e., Γ_{ii} terms) give an estimate of the photometry or the power at the input waveguides of the DBC. In Tab. 1, we compare the photometry imbalance applied to the input waveguide numbered 4 for different cases. We see that the imbalance is well predicted for an ideal case that assumes very high photons and noiseless detectors. The imbalance matches the theoretical values in the high and intermediate-photon regime, but in the low-photon regime, the imbalance has deviated. However, when the imbalance decreases by a factor of 100, neither the

*For a 14-bit CRED2 camera, this saturation value equals 16,384.

†In other words, an increase in the standard deviation of a quantity leads to a decrease in the precision.

Table 1. Comparison of photometry imbalance for various cases. The imbalance is defined as the power ratio of the 4th input WG to the remaining input WGs, assuming that the power at the remaining input WGs is equal. The ideal case (second column) assumes very high photon numbers with noiseless detectors. For the remaining three cases, photon noise and detector noise are taken into account. High-photon: 10^5 photons/pixel, Intermediate-photon: 10^4 photons/pixel and Low-photon: 10^3 photons/pixel.

Photometry imbalance	Ideal	High-photon	Intermediate-photon	Low-photon
1	0.99	0.98	0.88	0.65
0.5	0.50	0.51	0.56	0.81
0.1	0.10	0.11	0.19	0.41
0.01	0.01	0.02	0.12	0.37

intermediate nor the low-photon regime gives a reliable estimate. It is to be noted that the self-coherence terms or the power terms at the input waveguides are fundamental in calculating the retrieved visibilities and CP of a DBC. In Tab. 1, the self-coherence terms become inaccurate with lower photon numbers and increasing power imbalance at the input waveguides. For strongly affected photometries, i.e., in the low-photon regime and/or strong (e.g., order of magnitude) power imbalance, the reliability of the retrieved visibility amplitude and CP is in question.

5. CONCLUSION

In this proceeding, we briefly discussed the outcome and the results of our first on-sky experiment of an IO device containing 4-input pupil remappers, DBC, and 23-output coherent reformatters for which a pupil remapping experiment was performed at the WHT. We identified different noise sources that affected our on-sky visibilities. Here, we analyzed the case of power imbalance at the input waveguides along with a linear phase ramp. With respect to the experiment, the power imbalance situation at the input waveguides corresponds to, e.g., drifts in the coupling efficiency due to environmental effects or due to imperfect design or alignment of the optical setup, such as a mismatch between MLA and SM, preventing perfect 1:1 conjugation. Slow changes in the coupling efficiency resulting from an uncontrolled environment might also induce phase errors, which were simulated as a linear phase ramp at the input waveguides. From the results, it can be concluded that if we are operating the DBC at a high-photon regime, maintaining an input power imbalance of < 10 and considering realistic detectors, the accuracy of the retrieved visibility amplitude can reach ~ 99 %, along with the precision of CP reaching ~ 0.01 rad. However, in the low-photon regime, the visibilities are drastically affected because the retrieved photometries obtained from the DBC do not give a reliable assessment. These results conclude that a re-design of the pupil remapping experiment with higher throughput, balanced input injection of light, stability, and further on-sky tests of the DBC at the large-sized telescope would drastically improve the on-sky results. This would allow us to utilize the potential of ULI-based IO DBC components as beam combiners for pupil remapping and long-baseline interferometry at optical wavelengths.

6. ACKNOWLEDGEMENTS

This work was supported by the Deutsche Forschungsgemeinschaft (DFG) through project 326946494, "Novel Astronomical Instrumentation through photonic Reformatting (NAIR)" and through the BMBF Unternehmen Region grant 03Z22AN11. We want to thank OPTICON for providing financial support for some of us who were on-site during the sky test at the William Herschel Telescope. This work would have been incomplete if we did not mention Mr. Norberto Gonzales – the telescope operator, Dr. Chris Benn – the support astronomer, Éric Gendron, Jean-Tristan M. Buey, Fanny Chemla, Mathieu Cohen, Dr. Nazim A. Bharmal, Dr. Lisa F. Bardou, Dr. Lazar Staykov, Dr. James Osborn, Dr. Timothy J. Morris – the instrumentation scientists and engineers for their technical assistance during the sky tests at the William Herschel Telescope.

REFERENCES

[1] Fleischer, J. W., Segev, M., Efremidis, N. K., and Christodoulides, D. N., "Observation of two-dimensional discrete solitons in optically induced nonlinear photonic lattices," *Nature* **422**(6928), 147–150 (2003).

[2] Zhang, P., Egger, R., and Chen, Z., "Optical induction of three-dimensional photonic lattices and enhancement of discrete diffraction," *Opt. Express* **17**, 13151–13156 (Jul 2009).

[3] Garanovich, I. L., Sukhorukov, A. A., and Kivshar, Y. S., "Defect-free surface states in modulated photonic lattices," *Phys. Rev. Lett.* **100**, 203904 (May 2008).

[4] Fleischer, J. W., Bartal, G., Cohen, O., Manela, O., Segev, M., Hudock, J., and Christodoulides, D. N., "Observation of vortex-ring "discrete" solitons in 2d photonic lattices," *Phys. Rev. Lett.* **92**, 123904 (Mar 2004).

[5] Minardi, S. and Pertsch, T., "Interferometric beam combination with discrete optics," *Opt. Lett.* **35**, 3009–3011 (Sep 2010).

[6] Diab, M. and Minardi, S., "Modal analysis using photonic lanterns coupled to arrays of waveguides," *Opt. Lett.* **44**, 1718–1721 (Apr 2019).

[7] Minardi, S., "Photonic lattices for astronomical interferometry," *Monthly Notices of the Royal Astronomical Society* **422**, 2656–2660 (05 2012).

[8] Diener, R., Tepper, J., Labadie, L., Pertsch, T., Nolte, S., and Minardi, S., "Towards 3d-photonic, multi-telescope beam combiners for mid-infrared astrointerferometry," *Opt. Express* **25**, 19262–19274 (Aug 2017).

[9] Saviauk, A., Minardi, S., Dreisow, F., Nolte, S., and Pertsch, T., "3d-integrated optics component for astronomical spectro-interferometry," *Appl. Opt.* **52**, 4556–4565 (Jul 2013).

[10] Pedretti, E., Piacentini, S., Corrielli, G., Osellame, R., and Minardi, S., "A six-apertures discrete beam combiners for J-band interferometry," in [*Optical and Infrared Interferometry and Imaging VI*], Creech-Eakman, M. J., Tuthill, P. G., and Mérand, A., eds., **10701**, 316 – 325, International Society for Optics and Photonics, SPIE (2018).

[11] Nayak, A. S., Poletti, T., Sharma, T. K., Madhav, K., Pedretti, E., Labadie, L., and Roth, M. M., "Chromatic response of a four-telescope integrated-optics discrete beam combiner at the astronomical l band," *Opt. Express* **28**, 34346–34361 (Nov 2020).

[12] Minardi, S., "Nonlocality of coupling and the retrieval of field correlations with arrays of waveguides," *Phys. Rev. A* **92**, 013804 (Jul 2015).

[13] Thomson, R. R., Kar, A. K., and Allington-Smith, J., "Ultrafast laser inscription: an enabling technology for astrophotonics," *Opt. Express* **17**, 1963–1969 (Feb 2009).

[14] Perrin, G., Lacour, S., Woillez, J., and Thiébaut, É., "High dynamic range imaging by pupil single-mode filtering and remapping," *Monthly Notices of the Royal Astronomical Society* **373**, 747–751 (10 2006).

[15] Jovanovic, N., Tuthill, P. G., Norris, B., Gross, S., Stewart, P., Charles, N., Lacour, S., Ams, M., Lawrence, J. S., Lehmann, A., Niel, C., Robertson, J. G., Marshall, G. D., Ireland, M., Fuerbach, A., and Withford, M. J., "Starlight demonstration of the Dragonfly instrument: an integrated photonic pupil-remapping interferometer for high-contrast imaging," *Monthly Notices of the Royal Astronomical Society* **427**, 806–815 (11 2012).

[16] Harris, R. J., Tepper, J., Davenport, J. J., Pedretti, E., Haynes, D. M., Hottinger, P., Anagnos, T., Nayak, A. S., Alonso, Y. H., Deka, P. J., Minardi, S., Quirrenbach, A., Labadie, L., and Haynes, R., "NAIR: novel astronomical instrumentation through photonic reformatting," in [*Advances in Optical and Mechanical Technologies for Telescopes and Instrumentation III*], Navarro, R. and Geyl, R., eds., **10706**, 157 – 171, International Society for Optics and Photonics, SPIE (2018).

[17] Harris, R. J., Sharma, T. K., Davenport, J. J., Hottinger, P., Anagnos, T., Nayak, A. S., Quirrenbach, A., Labadie, L., Madhav, K. V., and Roth, M. M., "NAIR: Novel Astronomical Instrumentation through photonic Reformatting," in [*Advances in Optical and Mechanical Technologies for Telescopes and Instrumentation IV*], Navarro, R. and Geyl, R., eds., **11451**, 18 – 31, International Society for Optics and Photonics, SPIE (2020).

[18] Nayak, A. S., Piacentini, S., Sharma, T. K., Corrielli, G., Osellame, R., Labadie, L., Minardi, S., Pedretti, E., Madhav, K., and Roth, M. M., "Integrated optics-interferometry using pupil remapping and beam combination at astronomical H-band," in [*Advances in Optical Astronomical Instrumentation 2019*], Ellis, S. C. and d'Orgeville, C., eds., **11203**, 55 – 56, International Society for Optics and Photonics, SPIE (2020).

[19] Corrielli, G., Atzeni, S., Piacentini, S., Pitsios, I., Crespi, A., and Osellame, R., "Symmetric polarization-insensitive directional couplers fabricated by femtosecond laser writing," *Opt. Express* **26**, 15101–15109 (Jun 2018).

[20] Nayak, A. S., Sharma, T. K., Labadie, L., Piacentini, S., Corrielli, G., Osellame, R., Éric Gendron, Buey, J.-T. M., Chemla, F., Cohen, M., Bharmal, N. A., Bardou, L. F., Staykov, L., Osborn, J., Morris, T. J., Pedretti, E., Dinkelaker, A. N., Madhav, K. V., and Roth, M. M., "First on-sky results with an interferometric discrete beam combiner (DBC) at the William Herschel Telescope," in [*Optical and Infrared Interferometry and Imaging VII*], Tuthill, P. G., Mérand, A., and Sallum, S., eds., **11446**, 360 – 372, International Society for Optics and Photonics, SPIE (2020).

[21] Nayak, A. S., Labadie, L., Sharma, T. K., Piacentini, S., Corrielli, G., Osellame, R., Éric Gendron, Buey, J.-T. M., Chemla, F., Cohen, M., Bharmal, N. A., Bardou, L. F., Staykov, L., Osborn, J., Morris, T. J., Pedretti, E., Dinkelaker, A. N., Madhav, K. V., and Roth, M. M., "First stellar photons for an integrated optics discrete beam combiner at the william herschel telescope," *Appl. Opt.* **60**, D129–D142 (Jul 2021).

[22] Huby, E., Perrin, G., Marchis, F., Lacour, S., Kotani, T., Duchêne, G., Choquet, E., Gates, E. L., Woillez, J. M., Lai, O., Fédou, P., Collin, C., Chapron, F., Arslanyan, V., and Burns, K. J., "First, a fibered aperture masking instrument - i. first on-sky test results," *A&A* **541**, A55 (2012).

[23] Myers, R. M., Hubert, Z., Morris, T. J., Gendron, E., Dipper, N. A., Kellerer, A., Goodsell, S. J., Rousset, G., Younger, E., Marteaud, M., Basden, A. G., Chemla, F., Guzman, C. D., Fusco, T., Geng, D., Roux, B. L., Harrison, M. A., Longmore, A. J., Young, L. K., Vidal, F., and Greenaway, A. H., "CANARY: the on-sky NGS/LGS MOAO demonstrator for EAGLE," in [*Adaptive Optics Systems*], Hubin, N., Max, C. E., and Wizinowich, P. L., eds., **7015**, 52 – 60, International Society for Optics and Photonics, SPIE (2008).

[24] Gendron, E., Vidal, F., Brangier, M., Morris, T., Hubert, Z., Basden, A., Rousset, G., Myers, R., Chemla, F., Longmore, A., Butterley, T., Dipper, N., Dunlop, C., Geng, D., Gratadour, D., Henry, D., Laporte, P., Looker, N., Perret, D., Sevin, A., Talbot, G., and Younger, E., "Moao first on-sky demonstration with canary," *A&A* **529**, L2 (2011).